

P47 OBSERVATIONS OF HAILSTONE CHARACTERISTICS UTILIZING A NEW INSTRUMENTATION PLATFORM

Tanya M. Brown*

Insurance Institute for Business & Home Safety, Richburg, South Carolina

Ian M. Giammanco

Insurance Institute for Business & Home Safety, Richburg, South Carolina

D. Scott Robinett

Insurance Institute for Business & Home Safety, Richburg, South Carolina

1. INTRODUCTION

The Insurance Institute for Business & Home Safety (IBHS) is undertaking a multi-faceted research effort to study hailstorms with the goal of reducing property losses. As part of this effort, IBHS researchers are evaluating current impact testing standards for roofing products, and developing improvements to the test standards if warranted. A foundational element of this research effort is the characterization of damaging hail which is assumed to be a function of size, density, and hardness. IBHS conducted a pilot field project in the late spring of 2012 in an effort to quantify the hardness property of hailstones through in-situ measurements.

The general characteristics of hailstones and the climatological frequency of hail events have been well documented over the past several decades. There is much information regarding size, shape, and density of hailstones, yet little information exists regarding the hardness property of individual hailstones. Within historical literature, hailstones are often referred to as “soft”, “hard”, “spongy” or “slushy”, providing only a qualitative description of the hailstones (Bilhelm and Relf, 1937; Carte 1966; Knight and Knight 1973). It is hypothesized that the hardness property of a hailstone influences the damage produced upon impact.

Understanding this relationship is vital to ensuring that laboratory impact tests are improved and validated. It is understood that the microphysical mechanisms which govern hail growth within thunderstorms are complex, however identifying a link to a given set of environmental characteristics which may produce more damaging hail provides a critical step in risk modeling applications as well as in assessing the impact of climate change on severe hail events.

IBHS has developed a new instrumentation platform to measure the hardness property of hailstones by examining the compressive stress required to fracture an individual hailstone. The new instrument package was deployed for the first time during the 2012 field study. The primary objective was to collect compressive stress measurements of freshly fallen hailstones as well as their dimensions and mass. In addition, each stone was photographically cataloged. The secondary objective was to test the developed instrumentation, associated software, and experimental plans for use in modifying or developing a future, larger-scale hail field program. In addition, a third objective was to interrogate radar information and large scale environmental conditions to identify potential relationships in the identification and prediction of damaging hail.

*Corresponding Author Address: Tanya M. Brown, PhD. Insurance Institute for Business & Home Safety Research Center, 5335 Richburg Rd, Richburg SC 29729. tbrown@ibhs.org

2. INSTRUMENTATION

A unique, custom-designed instrument was developed by IBHS engineers, scientists, and technical staff to measure the compressive stress of a hailstone. The application of load cell technology made it possible to obtain a quantitative assessment of the hardness property of individual hailstones, by measuring the force required to fracture the hailstone. The device was originally developed for laboratory use, but was modified to make it more rugged and portable for use in the field. A photograph of the field instrument is provided in Figure 1. In addition to the compressive force measurements, the physical dimensions of each stone must be recorded, to allow for the calculation of compressive stress at fracture. The mass of each stone is also determined to provide an additional basis for comparing results.

The field measurement system consisted of four primary components. The first was a digital camera with GPS time and location capability for use in photographically cataloging each measured hailstone. The second piece of instrumentation was a caliper used to measure the dimensions of each stone. Each stone was also weighed using a digital scale. Hailstones were assumed to be a spheroid with two equal dimensions ($x_1 = x_2$) and a third dimension (y), illustrated in Figure 2. The dimensions x_1 and y were measured with the caliper. The final piece of instrumentation which made up the measurement system was the device used to measure the compressive force required to fracture each stone (i.e. "hardness"). The device consisted of a clamping handle in which the compressive force was incrementally increased until the point of fracture and a 227 kg (500 lb) capacity single axis load cell was attached to the bottom plate to measure the force applied to the stone. In order to collect and store the information, a unique piece of software was developed using National Instrument's (NI) LabVIEW. The electrical current information from the load cell was routed through a signal conditioning circuit board to

produce a voltage output. The voltage signal was acquired through a NI universal serial bus (usb) module for processing. In order to convert the voltage output into a compressive force value, the device was calibrated using known weights to develop a calibration function. The data acquisition graphical user-interface (gui) also allowed the user to enter each stone's dimensions, mass, and other deployment information such as storm type and a deployment identification number. The program also interfaced with a GPS unit to record the latitude and longitude of each data collection location. A conceptual diagram of the measurement system is provided in Figure 3.

3. METHODOLOGY

3.1 *Experimental Plans*

Experimental plans and procedures were developed and applied during field operations. The Great Plains region of the United States was selected as the project domain because this area offered good visibility and quality gridded road networks allowing for safe intercepts of severe thunderstorms. In addition, this region generally experiences more severe hail events than other parts of the U.S (Changnon et al. 2009).

Forecast preference was given to regions with the necessary conditions for supercell thunderstorms since this type of thunderstorm exhibits the highest probability for significant hail (Browning 1963; Browning 1977; Lemon and Doswell 1979; Doswell and Burgess 1993). Target storms were selected based on their radar presentation and the ambient environment in which they were embedded. This allowed for an estimate of the target storms' hail-producing potential. Additional regional and storm target preference was given to areas within upgraded dual-polarization WSR-88D coverage.

3.1.2 *Data Collection*

Idealized deployment and data collection strategies were developed for various storm types (e.g. supercell, squall line, multi-cell), road

networks, and number of teams. Teams were safely positioned in close proximity to the target storm but removed from the region of hail fall. As the target storm passed, teams would proceed to the region of hail fall to collect measurements. Two examples of data collection strategies are given in Figures 4 and 5. For a two team/one road deployment, one team attempted to collect data near the maximum hail fall (as indicated by radar and/or visually) while the other documented stones at the edges of the hail swath, as shown in Figure 4. If road networks allowed, a two team/two road deployment strategy could be executed with Team #2 positioning further downstream of Team #1 and the target storm. This experimental plan was developed to provide information on the spatial and temporal evolution of the swath of severe hail. Executing this experimental plan during the 2012 field study proved difficult due to unfavorable road networks and limitations in radio communications between the two teams. Typically, Team #2 remained tethered to Team #1 as a result of radio communication difficulties and a one road/one team deployment strategy was used (Figure 5).

All three team members were responsible for collecting a relatively representative sample of the range of stones found at each deployment location. However, it is unlikely that the sample size was representative of the mean storm-scale hail fall distribution and may not necessarily represent the true distribution at the given deployment site. One team member was then responsible for photographing each stone selected for measurement. GPS time, latitude, and longitude were included with the metadata for each picture. An example is provided in Figure 6. After each stone was photographed the second team member measured the dimensions and mass of each stone, and operated the hardness device, while the third operated the LabVIEW data acquisition script to log the dimensions and mass, and to ensure that the compressive force information was being acquired and stored correctly. Data collection periods typically ranged from 15-45 minutes and were dependent upon approaching convection

and the density of hail fall at a given deployment site.

3.2 Numerical Model and Radar Data

A series of environmental condition data, storm report data, and radar data were archived by WeatherPredict Consulting, Inc., for use in later analysis. The archived radar data included WSR-88D data for radar(s) beginning two hours prior to operations. The Level II full-volume moments and the Level III information were archived, this included dual-polarization data when applicable. The 00 UTC, 12 UTC, and any 18 UTC upper air soundings from the three stations closest to each deployment site were collected along with numerical model gridded initialization fields. The model datasets included the National Center for Environmental Prediction's (NCEP) Rapid Refresh (RAP) model, and the Earth System Research Laboratory's (ESRL) High-Resolution Rapid Refresh (HRRR) model initializations at 12 UTC and continuing hourly until operations were completed each day. In addition to radar and model data, local storm reports for each operation day were also cataloged.

4. DATA SUMMARY

A total of 12 datasets were collected from nine storms, all which exhibited supercell characteristics at some point in their lifecycle. The project featured seven operation days from May 25 through June 7, 2012. All storms were non-tornadic at the time in which they crossed the deployment roadway. Figure 7 shows the deployment locations and a summary of each is provided in Table 1.

The sizes of hailstones measured ranged from as small as 0.41 cm to as large as 7.75 cm. The majority of stones measured were generally disk-shaped or roughly spherical with a mean oblateness ($\frac{x_1 - y_1}{x_1}$) of 0.29 (Snyder 1987). It is noted that there were some irregularly-shaped stones that could not be considered a spheroid. Although some measured stones were smaller than the severe criteria, the majority (65%) of

stones had at least one dimension over the 2.54 cm (1 in) threshold for severe hailstones while 75% of the dataset exhibited diameters less than 4 cm. The probability distribution of measured diameters is provided in Figure 8.

The mean mass of the measured hailstones was 9.8 g with 90% of the dataset falling below 20 g. The distribution of measured hailstone mass is provided in Figure 9. The most massive stone measured was 124 g which was associated with the largest diameter measured. This stone had a diameter of over 7 cm and was found near Kingfisher, OK on 29 May 2012. The relationship between the measured diameter and mass was found to be in relative agreement with historical literature (Dennis et al. 1971) and exhibited an exponential increase in mass with diameter (Figure 10). The associated power-law fit explained 83% of the variance.

5. ANALYSIS

5.1 Scaling Analysis

The measured dimensions of each hailstone were examined in order to investigate the appropriate scaling variable for analyses of the compressive force data. As shown in Figure 11 (top-left), compressive force measurements exhibited a relationship with diameter such that larger stones typically required a larger compressive force in order to fracture the stone. A similar relationship was found with regards to mass (not shown).

The cross-sectional area and surface area assuming an oblate-spheroid shape were investigated for use in scaling the peak compressive force in order to arrive at a peak compressive stress. The equation for the surface area of an oblate spheroid is:

$$A_{oblate} = 2\pi a^2 \left(1 + \frac{1-e^2}{e} \tan^{-1} e\right) \quad (1)$$

where $e^2 = 1 - \frac{x_1^2}{y^2}$, x_1 and y are the dimensions shown in Figure 3 (Hilbert and Cohn-Vossen 1998). The peak compressive force exhibited a linear trend with surface area (Figure 11 bottom-

left) but this variable was excluded since the applied force is not uniform across the entire surface of the hailstone. The square of the diameter was also evaluated as a scaling variable (Figure 11 top-right) in order to present a pseudo-peak stress, with units of Pascals (N m^{-2}) in accordance with typical materials testing methodology (Beer and Johnston 1992; Meriam and Kraige 1998). This variable was ultimately not selected because the cross-sectional area (Figure 11) of the two measured dimensions was more appropriate to represent a compressive stress. Qualitative evidence from the field suggested that although the plane of fracture was not exactly along the cross-section through which the force was applied. It was roughly aligned, and both dimensions which make up that area were physically measured. Errors in the cross-sectional area are associated with the assumption that a hailstone is spheroidal. The peak stress (σ_c) is a function of the peak compressive force (F_c), the dimensions (x_1, y), and a coefficient of error (c) which accounts for cross-sectional error, which is unknown (Equation 2):

$$\sigma_c = \frac{F_c}{x_1 y c} \quad (2)$$

Therefore, the compressive force measurements were scaled by the cross-sectional area through which the force was applied ($x_1 y$). Additionally, the volume of each stone was calculated through the assumption of a spheroid shown by equation 3:

$$V = \frac{4}{3} \pi x_1^2 y c \quad (3)$$

Within subsequent density calculations, it was found that the two measured dimensions were inadequate for obtaining an accurate volume measurement and produced erroneous density values. The error is likely a result of the non-uniform nature of the surface of typical hailstones such that a percentage of the volume is effectively excluded through the use of the two specified dimensions. The use of an immersion test to obtain a volume measurement, used in historical literature, was considered impractical

in a field setting and renders the stone un-useable for compressive force testing (Knight and Heymsfeld 1983). For the analyses presented here, the peak compressive force at the point of fracture is scaled by the cross-sectional area to provide a peak compressive stress, which is used to represent the hardness property. It is noted that future work will investigate a more robust cross-sectional area approximation, additional scaling variables, and methodologies. It is vital to establish an accurate approach to estimating the compressive stress in order to derive a reliable proxy for the hardness of individual stones so that laboratory stones with similar ranges of hardness can be produced. Ultimately the hardness will affect the complex impact dynamics, including fracturing of the hailstone, of the stone with a roof cover, siding or some other object and the resulting damage.

5.2 Hardness properties of measured hail

The distribution of the peak compressive stress values during the 2012 pilot field study fit a Weibull distribution well (Figure 12). The mean compressive stress at fracture was 728 kPa with 75% of the measured stones having a compressive stress less than 790 kPa. A maximum compressive stress of 4317 kPa was observed during deployment 3B1 near Greenfield, OK (see Table 1) associated with a 1.6 cm diameter hailstone. The range of peak stress values generally fell within the range of those found by Field et al. (2010) when examining compressive stress versus strain relationships for pure ice cylinders at temperatures of -5 to -30 C. The limited but reasonable comparison was encouraging given the difficulty in evaluating the true cross-sectional area along the plane of fracture.

Observations were stratified by individual deployment and parent thunderstorm. When peak compressive stress values were examined as a function of mass, a storm dependency was observed for several events (Figure 13). Values were often clustered by deployment day with hailstones having similar values of peak stress

despite varying mass. Despite very complex microphysical hail growth processes, the result is somewhat expected given the general environmental influences on hail production (Fawbush and Miller 1952; Miller 1972; Kitzmiller and Briedenbach 1993; Doswell and Rasmussen 1994; Billet et al. 1997; Edwards and Thompson 1999; Jewell and Brimelow 2009).

5.3 Environmental influences

Historical literature has acknowledged the influence of the mesoscale and storm-scale environment on convective updraft organization, strength, and subsequent hail production (Browning and Foote 1976; Browning 1977; Knight 1984). It is often assumed that hail production and large hail sizes require strong updrafts and that maximum hail size is positively correlated with the updraft strength (Brandes et al. 1997). However, forecasting maximum hail size as well as quantity has proven to be quite difficult (Johns and Doswell 1982; Doswell et al. 1982). Historical methodologies have focused on using convective available potential energy (CAPE) and thermodynamic profiles of various layers aloft with limited success (Fawbush and Miller 1952; Foster and Bates 1956; Miller 1972; Renick and Maxwell 1977; Moore and Pino 1990). More recent work by Jewell and Brimelow (2009) coupling environmental characteristics through a cloud model with a hail growth model has shown promising results in estimating the maximum hail diameter. This provided motivation to examine the hardness property in a similar manner.

A proximity sounding approach was used to examine the convective environment for each sampled event. Rawinsonde profiles were selected based on their representativeness of the general storm inflow environment. This proved difficult for some cases where the closest sounding was contaminated by outflow from nearby convection. Each sounding was modified using the RAOB software for the closest observed surface temperature and dewpoint within the inflow region (Edwards and

Thompson 1998). The most unstable parcel path in the lowest 300 mb was used in accordance with Doswell and Rasmussen (1994). It is noted that this methodology may not accurately depict the true storm-scale environment; however it represents an appropriate operational forecast technique (Edwards and Thompson 1998).

The compressive stress was examined as a simple function of CAPE and freezing level as these quantities are often used operationally to estimate the probability of large hail. The compressive stress increased through CAPE values of 2500 J/kg before decreasing, as shown in Figure 14. The compressive stress exhibited little dependence on the height of the freezing level, with lower heights typically producing a smaller compressive stress at fracture. It is noted that a freezing level of 3750 m produced the peak compressive stress for the dataset which occurred with an estimated CAPE value of 2500 J/kg. Kitzmiller and Briedenbach (1993) suggested that lower freezing level heights limited hail exposure to melting temperatures and slowed the rate of melting. The limited data presented in this study would indicate that melting of stones may have little influence on the measured compressive stress required to fracture the stone.

The presence of both instability and vertical wind shear is understood to contribute the longevity and severity of convective storms (Marwitz 1972a; Chisolm and Renick 1972; Browning 1977; Wesiman and Klemp 1982, 1984, 1986; Sherwood 2000; Schultz et al. 2000). Given the promising results of Jewell and Brimelow (2009) in estimating the maximum hail size through the analysis of environmental conditions and a cloud and hail growth model, the energy shear index (ESI) was calculated for each proximity sounding. The index is the product of the surface-based CAPE and 1.5 – 6 km wind shear (Brimelow et al. 2002a). The index was applied as an indicator of updraft duration such that values greater than $5 \text{ m}^2 \text{ s}^{-2}$ yielded updraft durations greater than 60 minutes. The updraft duration was applied within a cloud and hail

growth model to produce maximum hail size estimates (Brimelow et al. 2002a). It is speculated that longer updraft durations may correspond to longer resident times which could influence the hardness property of hailstones. As shown in Figure 15, the peak compressive stress exhibited a general increase with ESI. All cases, except one, exhibited ESI values over 3. Although the sample size is quite small, the result is encouraging.

6. SUMMARY AND FUTURE WORK

The field study presented here represents the first in-situ measurements of the compressive stress required to fracture hailstones and is a first step in quantifying the hardness property of hail. Over 230 hailstones were measured and photographically cataloged over the seven operation days of the project. It is hypothesized that the hardness property of hail influences the impact related damage caused by hail striking different types of materials and systems.

Although the dataset is limited, it did indicate a general relationship that larger diameter hailstones typically require a larger amount of force to fracture them. In addition the mass of stones examined as a function of diameter exhibited a very well behaved exponential relationship and were in good agreement with historical literature. The assumption that stones were spheroidal was found to be problematic when computing the volume and subsequent density from the two dimensions measured. The non-uniformity of the surface of hailstones resulted in errors in the estimated volume of the stone. Selecting an appropriate scaling variable to evaluate the compressive stress at fracture was also difficult due to errors in the estimation of the cross-sectional area of the plane of fracture. However the use of the measured dimensions (x,y) to scale the compressive force measurements resulted in peak compressive stress values that were within the range of those found in a limited comparison of the compressive stress required to fracture pure ice cylinders (Field et al. 2010).

The large-scale environment for each case was examined through the use of proximity soundings to describe the available instability and vertical shear. The distribution of compressive stress measurements for each case was examined with respect to the ESI derived from the associated proximity sounding (Brimelow et al. 2002a). The ESI showed some promise in use as a predictive variable for hailstone hardness. The encouraging results of Jewell and Brimelow (2009) in forecasting maximum hail size and the probabilities of severe hail could be applied to the hardness property through associated mass and diameter relationships. Thus, improved estimates of the dimensions, volume, and density of measured stones are greatly needed to investigate the ability of the cloud and hail growth model to forecast the associated hardness property of hailstones. The storm-by-storm dependence also supported the hypothesis that the environment in which the storm is embedded influences the hardness of hailstones which reach the ground. It is also noted that hailstones collected from different storm-relative locations from the same parent thunderstorm typically exhibited similar hardness properties.

The dataset acquired during the project is a very small sample but illustrates that in-situ compressive stress measurements can be made. It also highlights the need for continued and improved measurements of hailstone characteristics. These measurements are vital to improving laboratory test methods and developing an understanding of the impact dynamics of a hailstone with specific characteristics and the resulting damage to different materials and systems.

7. Acknowledgments

The authors would like to thank the IBHS staff who participated in collecting the data presented in this study as well as the research laboratory technicians for assistance in developing the field instrument components. The authors would also like to acknowledge Dr. Dave Bachiochi and Dave Hamilton from WeatherPredict Consulting

Inc. for archival of radar data, model initialization fields, and local storm reports during the field project.

8. REFERENCES

Beer, F.P., and E.R. Johnston, 1992: *Mechanics of Materials*. McGraw-Hill, 717 pp.

Bilhelm, E.G., and E.F. Relf, 1937: The dynamics of large hailstones. *Quart. J. Roy. Meteor. Soc.*, **63**, 149-162.

Billet, J., M. DeLisi, and B.G. Smith, 1997: Use of regression techniques to predict hail size and the probability of large hail. *Wea. Forecasting*, **12**, 154-164.

Brandes, E., J. Vivekanadan, J. Tuttle, and G. Kessinger, 1997: Hail production in Northeast Colorado hailstorms, *Proceedings 27th Conference on Radar Meteorology*, Amer. Meteor. Soc., Boston, MA, 527-530.

Brimelow, J.C., T.W. Krauss, and G.W. Reuter, 2002: Operational forecasts of maximum hailstone diameter in Mendoza, Argentina. *J. Wea. Mod.*, **34**, 8-17.

Browning, K.A., 1963: The growth of large hail within a steady updraught. *Quart. J. Roy. Meteor. Soc.*, **89**, 490-506.

Browning, K.A., 1977: The structure and mechanisms of hailstorms: *A review of hail science and suppression*, *Meteor. Monogr.*, No. 38, Amer. Meteor. Soc., 1-43.

Browning, K.A. and G.B. Foote, 1976: Airflow and hail growth in supercell storms and some implications for hail suppression. *Quart. J. Roy. Meteor. Soc.*, **102**, 499-533.

Carte, A.E., 1966: Features of Transvaal hailstones. *Quart. J. Roy. Meteor. Soc.*, **92**, 290-296.

Changnon, S.A., D. Changnon, and S.D. Hilberg, 2009: Hailstorms across the nation: An atlas about hail and its damages. Illinois State Water Survey Contract Report 2009-12, 78 pp.

Chisolm, A.J., and J.H. Renick, 1972: The kinematics of multi-cell and supercell Alberta hailstorms. Research Council of Alberta Hail Studies Rep. 72-2, 24-31.

- Dennis, A.S., P.L. Smith Jr., G.A.P. Peterson, and R.D. McNeil, 1971: Hailstone size distributions and equivalent radar reflectivity factors computed from hailstone momentum records. *J. Appl. Meteor.*, **10**, 79–85.
- Doswell III, C.A. and D.W. Burgess, 1993: Tornadoes and tornadic storms: A review of conceptual models. *The Tornado: Its Structure, Dynamics, Prediction, and Hazards, Geophys. Monogr.*, No. 79, Amer. Geophys. Union, 161-172.
- Doswell III, C.A. and E.N. Rasmussen, 1994: The effect of neglecting the virtual temperature correction on CAPE calculation. *Wea. Forecasting*, **9**, 625-629.
- Edwards, R. and R.L. Thompson, 1998: Nationwide comparisons of hail size with WSR-88D vertically integrated liquid water and derived thermodynamic sounding data. *Wea. Forecasting*, **13**, 277-285.
- Fawbush, E.J., and R.C. Miller, 1953: A method for forecasting hailstone size at the earth's surface. *Bull. Amer. Meteor. Soc.*, **34**, 235-244.
- Field, P.R., W. Hand, G. Cappelluti, A. McMillan, A. Foreman, D. Stubbs, and M. Willows, 2010: *Hail threat standardization*. European Aviation Safety Agency, Technical Report EASA.2008/5. 130 pp.
- Foster, D.S. and F.C. Bates. 1956: A hail-size forecasting technique. *Bull. Amer. Meteor. Soc.*, **37**, 135-140.
- Hilbert, D. and Cohn-Vossen, S. 1999: *Geometry and the Imagination*. Chelsea, 357 pp.
- Jewell, R., and J.C. Brimelow, 2009: Evaluation of Alberta hail growth model using severe hail proximity soundings from the United States. *Wea. Forecasting*, **24**, 1592–1609.
- Johns, R.H., and C.A. Doswell III, 1992: Severe local storms forecasting. *Wea. Forecasting*, **7**, 588-612.
- Kitzmler, D.H., and J.P. Briedenbach, 1993: Probabilistic nowcasts of large hail based on volumetric reflectivity and storm environmental characteristics. Preprints, *26th Conf. On Radar Meteorology*, Norman, OK, Amer. Meteor. Soc., 157-159.
- Knight, C.A., and N.C. Knight, 1973: Quenched, spongy hail. *J. Atmos. Sci.*, **30**, 1665-1671.
- Knight, N. C., and A. J. Heymsfield, 1983: Measurement and interpretation of hailstone density and terminal velocity. *J. Atmos. Sci.*, **40**, 1510–1516.
- Knight, C.A., 1984: Radar and other observations of two vaulted storms in northeast Colorado. *J. Atmos. Sci.*, **41**, 258-271.
- Lemon, L.R., and C.A. Doswell III, 1979: Severe thunderstorm evolution and mesocyclone structure as related to tornadogenesis. *Mon. Wea. Rev.*, **107**, 1184-1197.
- Marwitz, J.D., 1972: The structure and motion of severe hail storms. Part I: Supercell storms. *J. Appl. Meteor.*, **11**, 166-179.
- Meriam, J.L. and L.G. Kraige, 1998: *Engineering Mechanics Dynamics*. Wiley and Sons Inc., 723 pp.
- Miller, R.C., 1972: Notes on analysis of severe storm forecasting procedures of the Air Force Global Weather Center. *AFGWG Technical Report No. 200 (Rev)*, Air Weather Service, Scott Air Force Base, 190 pp.
- Moore, J.T., and J.P. Pino, 1990: An interactive method for estimating maximum hailstone size from forecast soundings. *Wea. Forecasting*, **5**, 508-525.
- Renick, J.H., and J.B. Maxwell, 1977: Forecasting hailfall in Alberta. *Hail: A Review of Hail Science and Hail Suppression, Meteor. Monogr.*, No. 38, Amer. Meteor. Soc., 145–151.
- Schultz, D.M., P.N. Schumacher, and C.A. Doswell III, 2000: The intricacies of instability. *Mon. Wea. Rev.*, **128**, 4143-4148.
- Sherwood, S.C., 2000: On moist instability. *Mon. Wea. Rev.*, **128**, 4139-4142.
- Snyder, J. P., 1987: *Map Projections--A Working Manual*. U. S. Geological Survey Professional Paper 1395. Washington, DC: U. S. Government Printing Office.
- Weisman, M.L. and J.B. Klemp, 1982: The dependence of numerically simulated convective

storms on vertical wind shear and buoyancy. *Mon. Wea. Rev.*, **110**, 504-520.

Weisman, M.L. and J.B. Klemp, 1984: The structure and classification of numerically simulated convective storm in directionally-varying wind shears. *Mon. Wea. Rev.*, **112**, 2479-2498.

Weisman, M.L. and J.B. Klemp, 1986: Characteristics of isolated convective storms. *Mesocale Meteorology and Forecasting*, P.S. Ray Ed., Amer. Meteor. Soc., 331-358.

Table 1: Data summary for each deployment.

Deployment ID	Date	Location	Dual-Pol Coverage	No. stones measured	Max. stone dimension (cm)	Mean stone dimension (cm)	Min. stone dimension (cm)	Max. compressive stress (kPa)	Mean compressive stress (kPa)	Min. compressive stress (kPa)
1A1	05/27/2012	Ravenna, NE	No	5	1.93	1.35	0.84	1326.5	877	711.7
2A1	05/28/2012	Lindsay, OK	No	32	4.75	2.77	1.14	2208.1	892	184.3
3A1	05/29/2012	Kingfisher, OK	KVNX	20	7.75	2.31	0.41	3713.9	1244	132.2
3B1	05/29/2012	Greenfield, OK	KVNX	17	3.05	1.93	0.61	4317.0	1310	270.7
4A1	06/01/2012	Channing, TX	KAMA	45	3.12	1.80	0.71	4197.4	853	160.3
5A1	06/02/2012	Eads, CO	No	17	3.33	1.63	0.53	759.2	389	185.7
6A1	06/06/2012	Remmington Ranch, WY	No	16	3.07	2.03	1.22	477.0	199	107.5
6A2	06/06/2012	Remmington Ranch, WY	No	20	3.23	2.57	1.65	541.8	231	59.4
7A1	06/07/2012	Cheyenne, WY	No	8	3.76	3.12	1.85	639.4	381	199.7
7B1	06/07/2012	Cheyenne, WY	No	14	3.66	2.44	1.42	2765.9	680	127.3
7B2	06/07/2012	Cheyenne, WY	No	35	5.41	3.25	1.83	751.7	497	262.3
7B3	06/07/2012	Cheyenne, WY	No	10	4.45	3.38	2.34	783.0	527	186.7

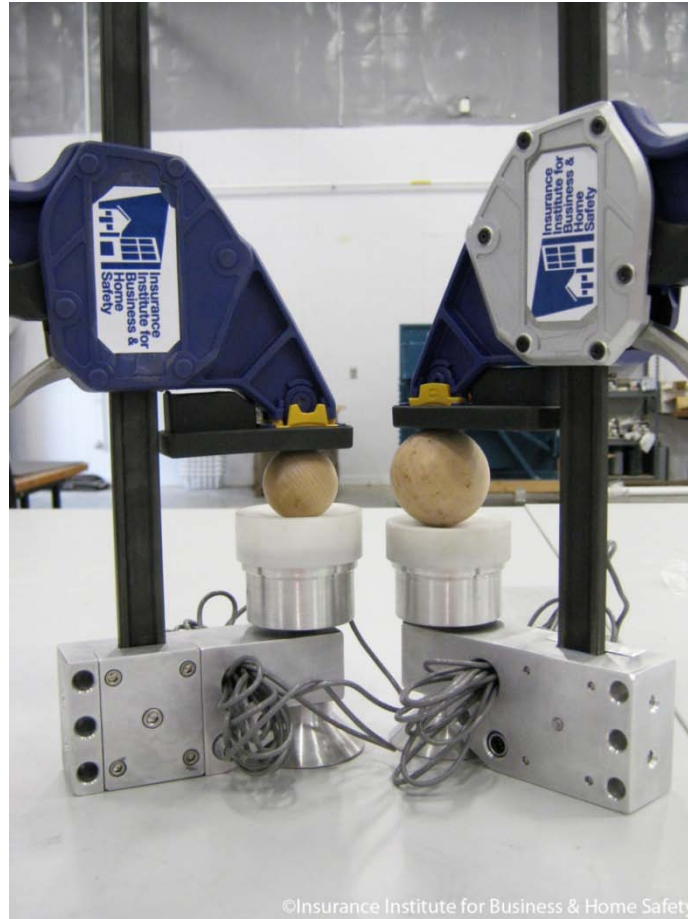


Figure 1: Photograph of the two prototype field compressive force measurement instruments.

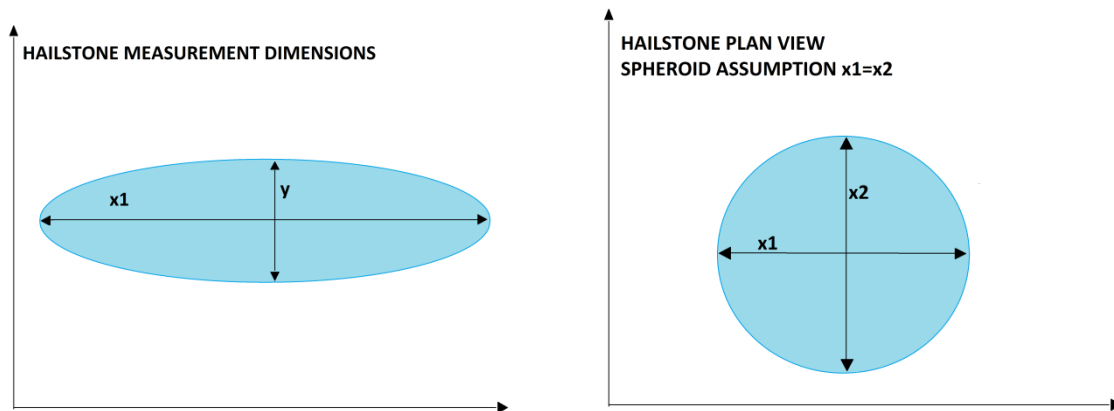


Figure 2. Diagram of the measured dimensions of hailstones. Each stone was assumed to be a spheroid in shape with dimensions x_1 and x_2 equal. Only dimensions x_1 and y were measured in the field.

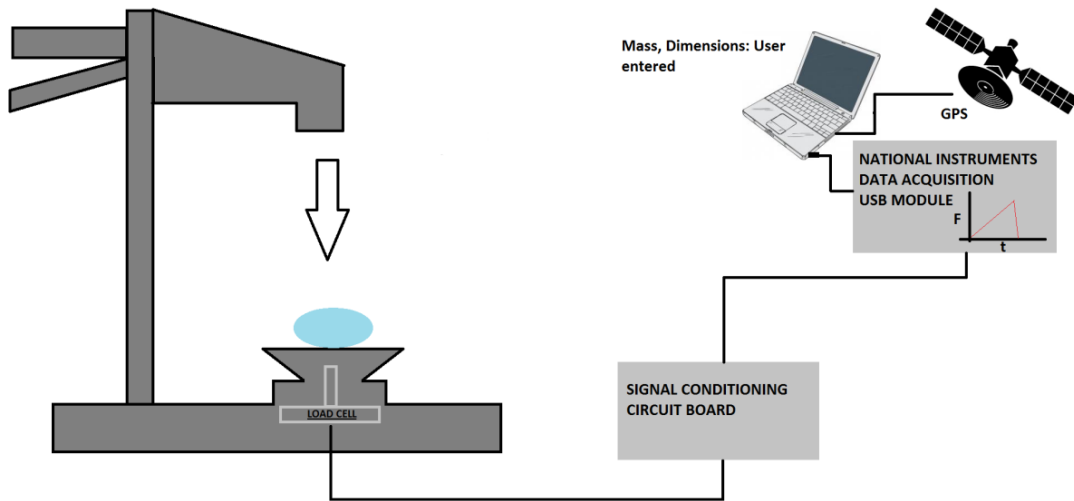


Figure 3: Conceptual diagram of the hailstone measurement system.

SUPERCELL

2 Team – One Road Deployment

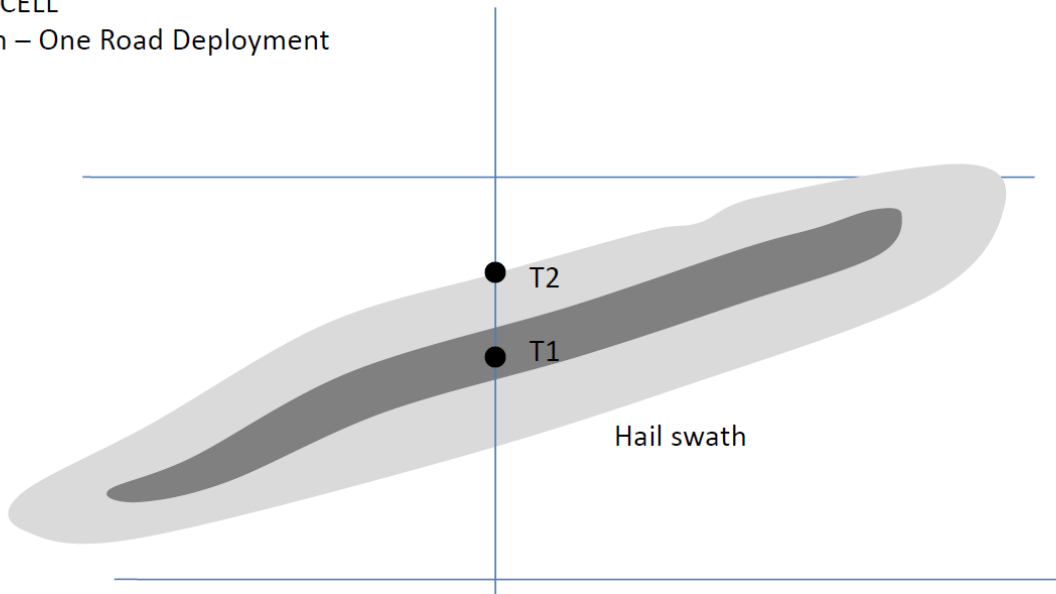


Figure 4: Two team/one road deployment strategy for a supercell thunderstorm.

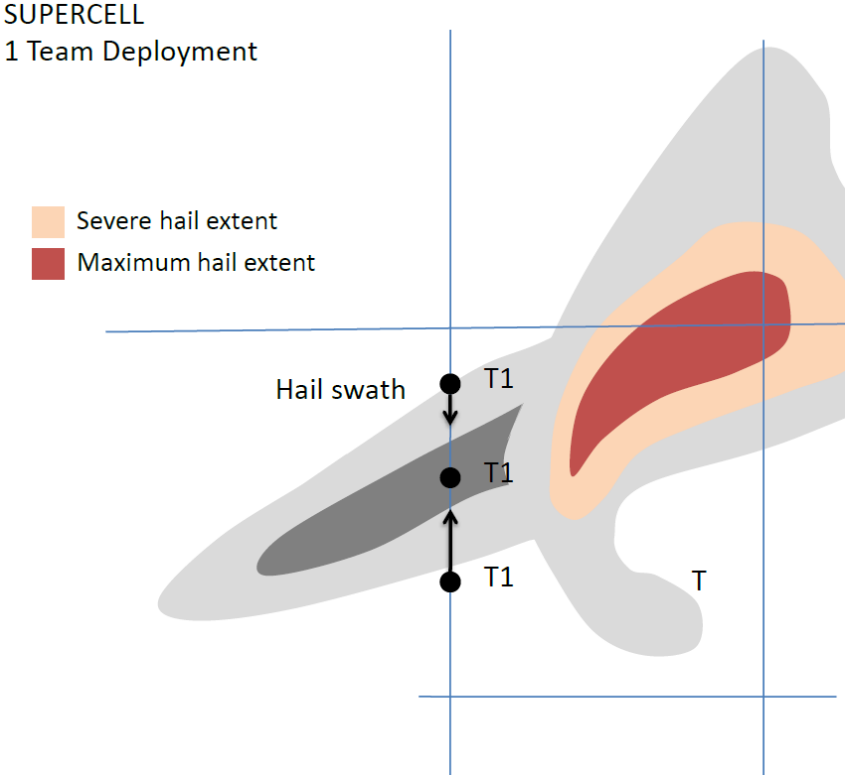


Figure 5: One team/one road deployment strategy for a supercell thunderstorm. This deployment strategy was often used with Team #2 tethered to Team #1 due to radio communication issues.



Figure 6: Photograph of a measured hailstone collected on 7 June 2012 near Cheyenne, WY.

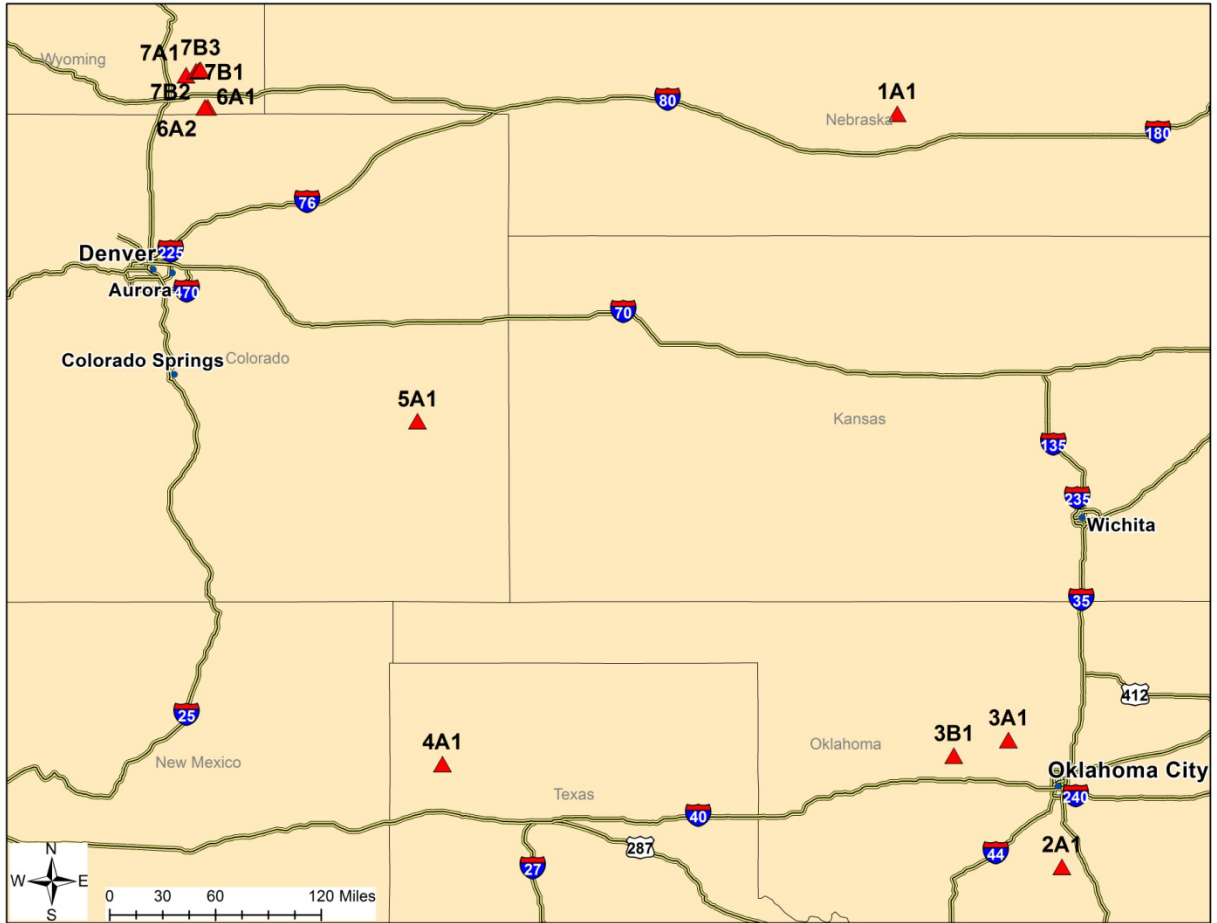


Figure 7: Deployment locations from the 2012 field campaign.

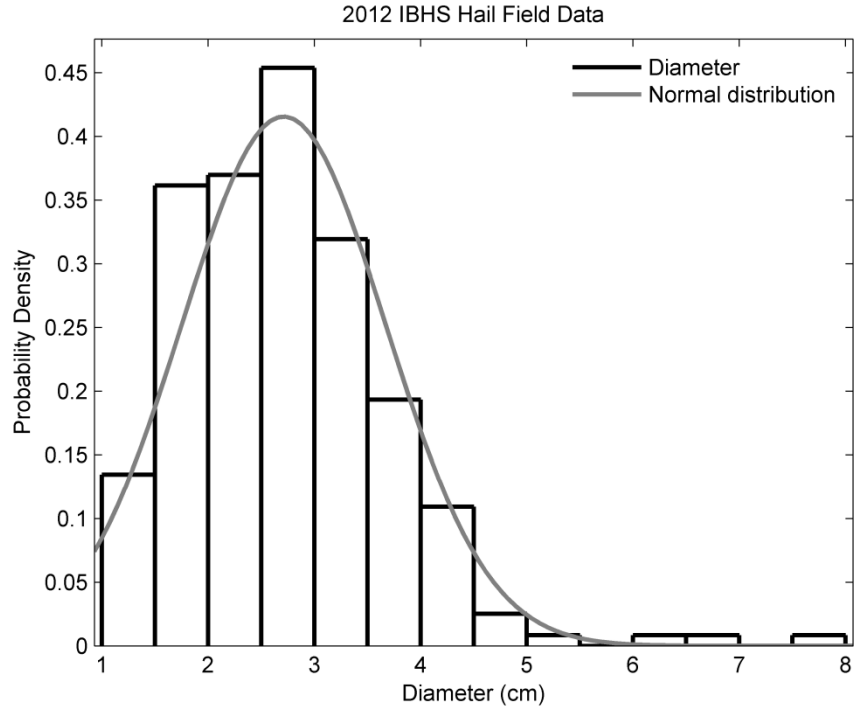


Figure 8: Probability distribution of measured hailstone diameters. The fitted normal distribution is provided (gray).

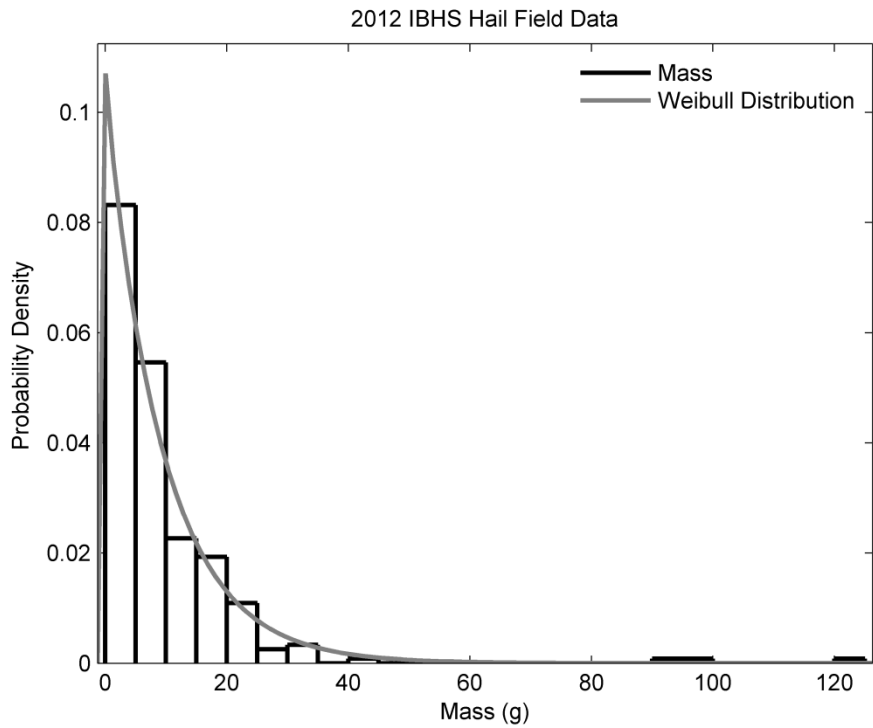


Figure 9: Probability distribution of the mass of hailstones measured. The fitted Weibull distribution is provided (gray).

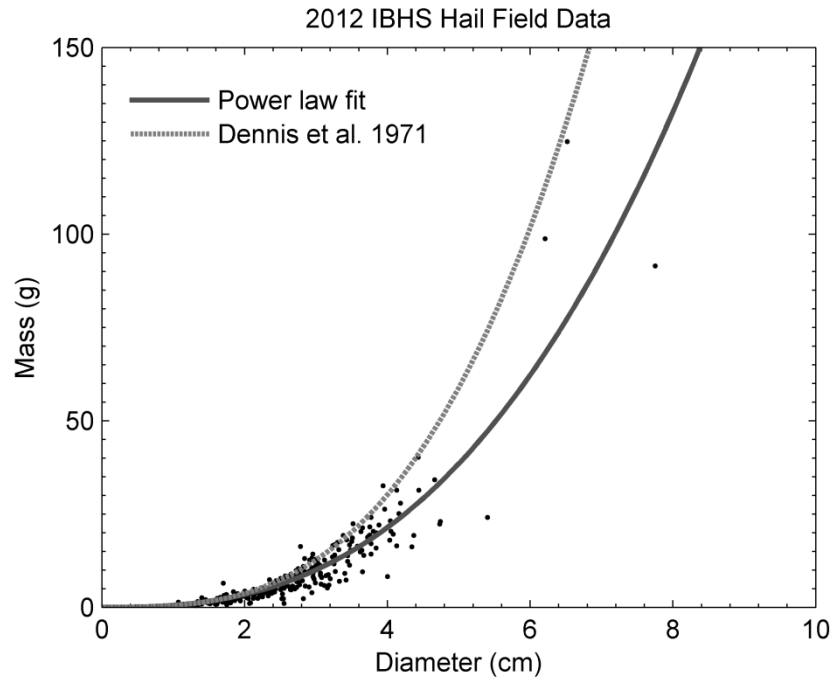


Figure 10: Mass of each hailstone measured shown as a function of diameter. A power-law least-squares fit is shown (solid) and the exponential model of Dennis et al. (1971) is also provided (dashed).

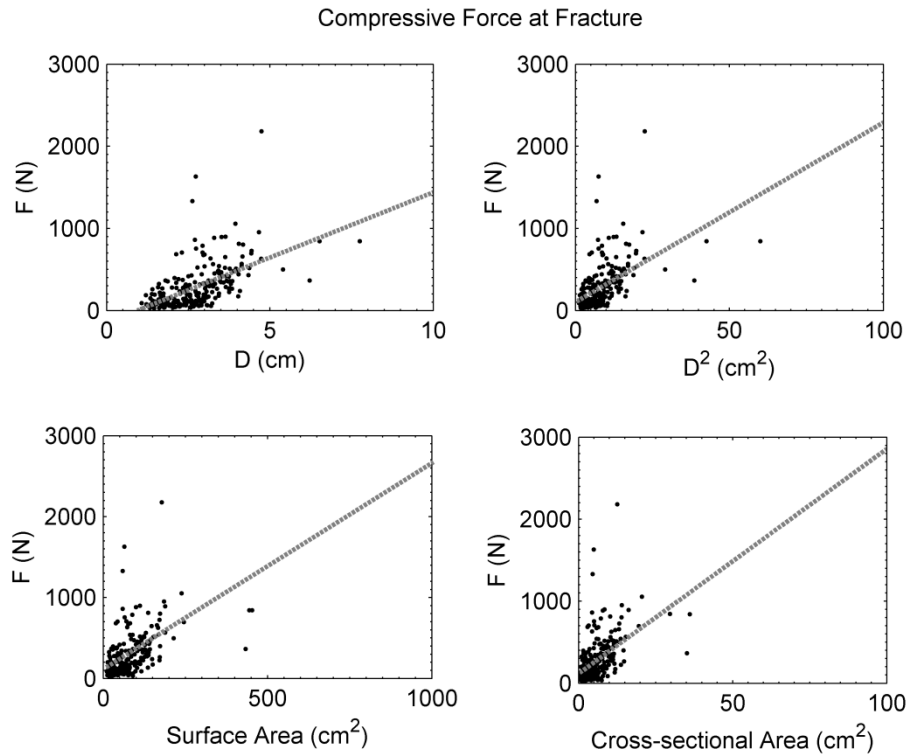


Figure 11: Peak compressive force for measured hailstones shown as a function of diameter (top-right), square of the diameter (top-left), cube of the diameter (bottom-left), and estimated cross-sectional area (bottom-right). A linear fit is also provided (dashed).

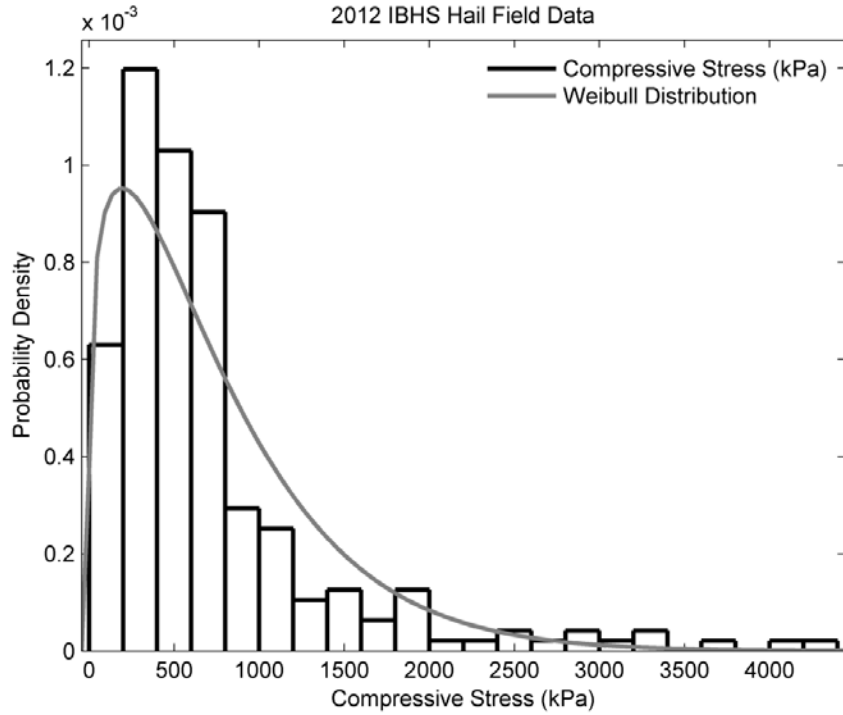


Figure 12. Probability distribution for measured compressive stress at fracture. A fitted Weibull distribution is provided (gray).

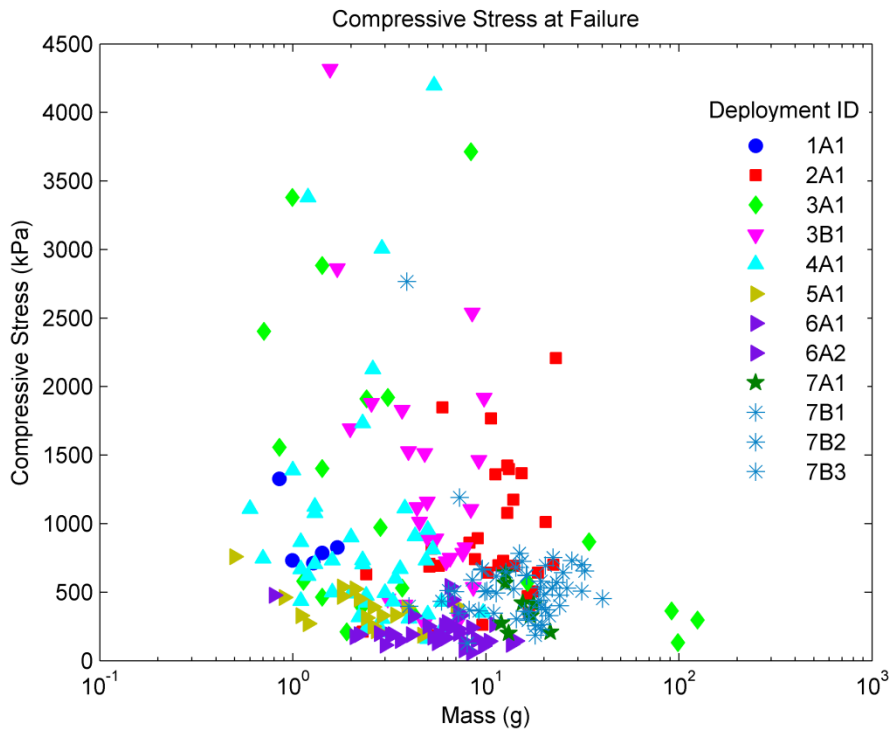


Figure 13. Compressive stress at fracture shown as a function of mass. Data are stratified by deployment identification number which is provided in the legend (see Table 1).

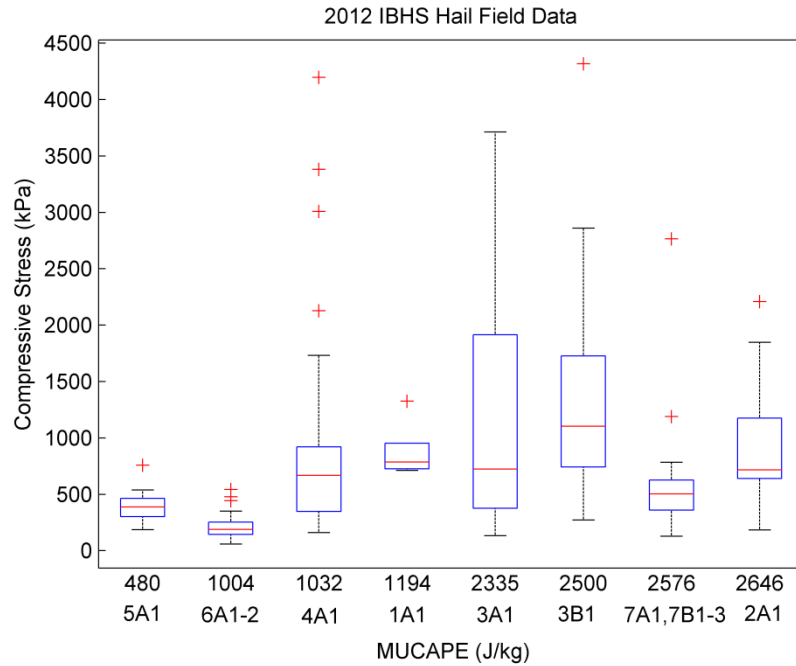


Figure 14. Boxplot of the distribution of compressive stress at fracture shown as a function of the CAPE for the most unstable parcel in the lowest 300 hPa of a modified proximity soundings for each deployment. The deployment ID included in each distribution is also provided.

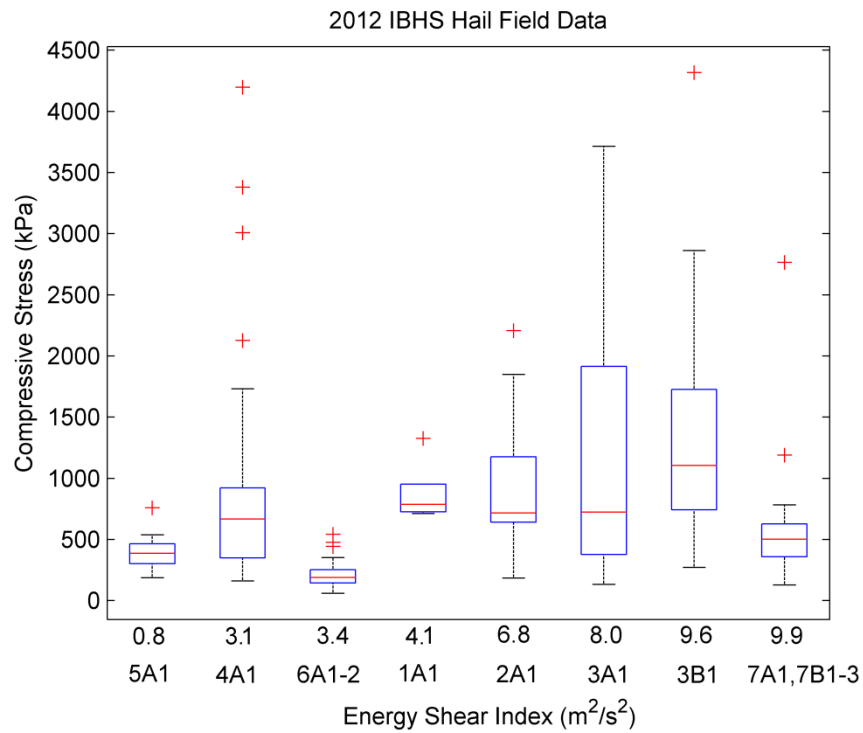


Figure 15. Boxplot of the distribution of compressive stress at fracture shown as a function of energy shear index. The deployment ID included in each distribution is also provided.